

Imaging Nanoprobe for Prediction of Outcome of Nanoparticle Chemotherapy by Using Mammography¹

Efstathios Karathanasis, PhD
Sankararaman Suryanarayanan, PhD, MBA
Sri R. Balusu
Kathleen McNeeley, MS
Ioannis Sechopoulos, PhD
Andrew Karellas, PhD²
Ananth V. Annapragada, PhD
Ravi V. Bellamkonda, PhD

Purpose:

To prospectively predict the effectiveness of a clinically used nanochemotherapeutic agent by detecting and measuring the intratumoral uptake of an x-ray contrast agent nanoprobe by using digital mammography.

Materials and Methods:

All animal procedures were approved by the institutional animal care and use committee. A long-circulating 100-nm-scale injectable liposomal probe encapsulating 155 mg/mL iodine was developed. Preliminary studies were performed to identify the agent dose that would result in adequate tumor enhancement without enhancement of the normal vasculature in rats. This dose was used to image a rat breast tumor ($n = 14$) intermittently for 3 days by using a digital mammography system; subsequently, the animals were treated with liposomal doxorubicin. The predictive capability of the probe was characterized by creating good- and bad-prognosis subgroups, on the basis of tumor enhancement found during imaging, and analyzing the tumor growth after treatment of the animals in these two subgroups.

Results:

A dose of 455 mg of iodine per kilogram of body weight was found to produce an undetectable signal from the blood while achieving enough intratumoral accumulation of the probe to produce adequate signal for detection. The good- and bad-prognosis subgroups demonstrated differential tumor growth rates ($P < .003$). An inverse linear relationship between the contrast enhancement rate constant during imaging and the tumor growth rate constant during treatment was found (slope = -0.576 , $R^2 = 0.838$).

Conclusion:

In this animal model, quantitative measurement of vascular permeability enabled prediction of therapeutic responsiveness of tumors to liposomal doxorubicin.

© RSNA, 2009

¹ From the Wallace H. Coulter Department of Biomedical Engineering, Georgia Institute of Technology/Emory University, 3108 UA Whitaker Bldg, 313 Ferst Dr, Atlanta, GA 30332 (E.K., S.R.B., K.M., R.V.B.); Department of Radiology and Winship Cancer Institute, Emory University, Atlanta, Ga (S.S., I.S., A.K.); and School of Health Informatics, University of Texas Health Science Center, Houston, Tex (A.V.A.). Received May 6, 2008; revision requested June 17; final revision received July 16; accepted August 4; final version accepted August 14. Supported by the Georgia Cancer Coalition (R.V.B.) and the National Science Foundation and Bioengineering and Environmental Systems grant 0401627 (R.V.B.). **Address correspondence** to R.V.B. (e-mail: ravi@gatech.edu).

The contents of this article are solely the responsibility of the authors and do not necessarily represent the official views of the National Science Foundation or the Georgia Cancer Coalition.

² **Current address:** Department of Radiology, University of Massachusetts Medical School, Worcester, Mass.

Nanoscale therapeutic interventions are increasingly important elements of cancer therapy (1,2). Nanoparticles (3,4) can be effective delivery vehicles for toxic chemotherapeutic drugs, increasing delivery efficiency to the targeted tumor while reducing off-target delivery (5). Liposomal anthracyclines were the first nanotherapeutic agents to be approved for clinical use as the first line for treatment of AIDS-related Kaposi sarcoma and relapsed ovarian cancer (6) and are under investigation in numerous clinical trials (128 active studies) for treatment of many types of cancer, especially breast cancer, which accounts for 41 active clinical trials (7).

In addition to the cytotoxic effect of the drug at the molecular level, the success of systemically delivered nanotherapeutic agents for solid tumors is critically dependent on the access that these agents have to tumors through the so-called leaky vasculature of the tumor microvasculature network. This network consists of an

immature blood microvessel system, with hypervascularization, abnormal vascular architecture, increased leakage through the vessel wall, and lack of lymphatic drainage (8,9). Nanoparticles preferentially accumulate in solid tumors by means of passive convective transport through leaky endothelium (extravasation) that is caused by pores varying from approximately 100 to 800 nm (10–12). The phenomenon is termed the *enhanced permeation and retention effect*. To date to our knowledge, there exist no clinical tools to determine whether tumor blood vessels are permeable to nanoparticles in this fashion. For instance, the current clinical protocols for liposomal doxorubicin consist of a standard dose every 3–4 weeks (13). No prior knowledge of tumor vessel status, especially leakiness, is taken into account for the dose scheduling. However, it is well known that the degree of tumor vasculature leakiness differs not only among same-type tumors but even spatially in the same tumor (14–16).

Our purpose was to prospectively predict the effectiveness of a clinically used nanochemotherapeutic agent by detecting and measuring the intratumoral uptake of an x-ray contrast agent nanoprobe by using digital mammography.

Materials and Methods

The contrast agent formulation used in this study is similar to one that has been licensed to a start-up company, Marval Biosciences (Houston, Tex), founded by two authors (A.V.A. and R.V.B.).

Implication for Patient Care

- An a priori determination of the extent of tumor vascular permeability to nanoparticle-based therapy can facilitate personalized therapy and spare potential nonresponders from the rigors of a chemotherapeutic regimen.

Fabrication of the Nanoscale X-ray Probe

A highly concentrated iodine solution (650 mg of iodine per milliliter) was prepared by dissolving iodixanol powder (lyophilized from Visipaque 320; GE Healthcare, Milwaukee, Wis) in pure water, with stirring and heating at 70°C. The rest of the procedures (E.K., with 7 years of experience in nanoparticle fabrication) were similar to those described previously (17). The liposomal probe contained 72 mg/mL of lipids and 155 mg/mL of iodine, and 100% of the iodine was encapsulated within the liposomes. The mean diameter of the liposomes was 96 nm (standard deviation, 8 nm), a size known to prevent renal clearance. An in vitro leakage experiment against isotonic phosphate-buffered saline exhibited very low leakage of the encapsulated iodine (<5% of the initial payload) during 3 days.

Animal Model

All animal procedures were approved by the institutional animal care and use committee at Georgia Institute of Technology, Atlanta, Ga. Our study took place from February 15, 2007, to December 10, 2007. A 0.2-mL aliquot containing 10^6 cancer cells (13762 MAT B III cell line; American Type Culture Collection, Manassas, Va), a mammary adenocarcinoma, was subcutaneously injected into the right flank of 53 8–9-week-old female Fisher rats (Harlan, Indianapolis, Ind). Caliper measurements were used to estimate tumor size, and the tumor volume, V_{tumor} , was calcu-

Advances in Knowledge

- Imaging studies of a rat breast tumor model by using a clinical digital mammography system resulted in identification of a dose of a long-circulating 100-nm-scale liposomal probe containing a high concentration of iodinated contrast agent (155 mg/mL) that produced undetectable signal from the blood while the accumulation of the agent in the tumor produced adequate signal for detection.
- Imaging of the extravascular intratumoral accumulation of the nanoprobe allowed detection and quantification of the tumor vascular permeability, which varied among animals.
- The imaging measurements of the tumor vascular permeability to the nanoprobe allowed prediction of the effect of a subsequent treatment with liposomal doxorubicin of similar composition and particle size as the nanoprobe.

Published online

10.1148/radiol.2502080801

Radiology 2009; 250:398–406

Author contributions:

Guarantors of integrity of entire study, E.K., A.V.A., R.V.B.; study concepts/study design or data acquisition or data analysis/interpretation, all authors; manuscript drafting or manuscript revision for important intellectual content, all authors; manuscript final version approval, all authors; literature research, E.K., S.S., S.R.B., K.M., A.K., A.V.A., R.V.B.; experimental studies, E.K., S.S., S.R.B., K.M., I.S., A.K., R.V.B.; statistical analysis, E.K., A.V.A.; and manuscript editing, all authors

See Materials and Methods for pertinent disclosures.

lated as follows: $V_{\text{tum}} = (d_1^2 \cdot d_2)/2$, where d_1 and d_2 are the minimum and maximum diameters (E.K., with 6 years of experience in animal handling and procedures).

X-ray Imaging

Imaging was performed by using a clinical digital mammography system (Senographe 2000D; GE Healthcare) (S.S. and I.S., with 10 and 6 years of experience in medical physics, respectively). To maximize the number of photons with energies above the k edge of iodine (approximately 33.2 keV) (18), imaging was performed at 49 kVp and 63 mAs by using a rhodium target and the available 25- μm -thick rhodium filter, with an added 0.254-mm-thick copper filter (19). The resultant x-ray spectrum was estimated by using a simulation program (XSPECT; Henry Ford Health Systems, Detroit, Mich), which uses semiempirical models (20).

To estimate the radiation dose to the animals during imaging, a previously validated Monte Carlo simulation for dosimetry studies (21) was modified to include a simplified version of the animal geometry (I.S.). In the simulation, a rat was represented as a 10-cm-long cylinder of water with a 4-cm diameter. To estimate the dose to the cylinder from the x-ray spectrum used in the imaging studies, the Monte Carlo simulation was performed repeatedly with monochromatic x-rays with energies from 20 to 49 keV in 0.5-keV steps. To achieve the necessary statistical accuracy, 1 million photons per energy level were simulated. The monochromatic results were combined with the x-ray spectrum obtained with the simulation program by using the method described by Boone (22).

Preliminary Dose Study

Initially, pilot imaging sessions were performed to determine the appropriate dose of the probe that would result in appropriate tumor enhancement with no detectable enhancement of the vasculature in rats. For this task, 16 animals were injected with the probe at doses that resulted in iodine concentrations in the blood that ranged from 6 to

20 mg/mL, with 2 mg/mL intermediate steps (two animals per dose), and were subsequently imaged at times of 0.5, 1, 5, and 10 minutes and of 24, 72, and 120 hours. From the acquired images, the dose threshold level above which the vasculature was not highlighted was identified with visual inspection by two reviewers in consensus (E.K., S.S.).

Effectiveness Prediction Study

At day 6 after tumor inoculation (tumor volume, approximately 300 mm^3), 14 animals were imaged before (0 minutes) and at defined times after (2 and 30 minutes and 24 and 72 hours) intravascular injection of the probe at the dose identified in the preliminary dose study. As a control for the imaging portion of the study, six animals that were also inoculated with the tumor but received an injection with 0.5 mL of saline only were imaged at the same times. Immediately after the last imaging session (at day 9 after tumor inoculation), the animals received an intravascular injection with liposomal doxorubicin at a dose of 10 mg/kg doxorubicin. As a control for the treatment portion of the study, 15 animals that underwent the same tumor inoculation and probe injection at the same times as the study group did not receive an injection with liposomal doxorubicin. Liposomal doxorubicin was prepared by following established methods (23). The tumor growth in each animal was monitored every day by using caliper measurements. The maximum size that tumors were allowed to grow was 3 cm. When the tumor reached 3 cm in diameter or when animals showed any signs of pain, prostration, labored breathing, sunken eyes, any skin ulcers, emaciation or anorexia, the animals were immediately euthanized by using a CO_2 chamber. Otherwise the animals were euthanized 21 days after tumor inoculation.

Image Analysis

The sequential image acquisitions provided the dynamics of the probe's intratumoral accumulation over time. The gray levels were measured in raw

data (Digital Imaging and Communications in Medicine format) by using software (ImageJ; National Institutes of Health, Bethesda, Md). An ellipsoid region of interest was used for the measurements surrounding the entire tumor lesion (E.K.), and the average value of the gray levels in the region of interest was used as the tumor enhancement. Because mammography is not a tomographic modality, the observed tumor enhancement represents the summation of the absolute enhancement caused by the contrast agent and the enhancement of overlying tissue structures. To normalize with respect to the overlying tissues, relative enhancement was computed by subtracting the enhancement value before contrast agent administration (time, 0 minutes) from the enhancement value after contrast agent administration (time, >0 minutes). Tumors that presented a relative enhancement of less than 50 digital units on the 24-hour postinjection image were assigned to the bad-prognosis subgroup, whereas tumors with a relative enhancement of 50 digital units or more were assigned to the good-prognosis subgroup.

As a control, the relative enhancement of a normal section of tissue was also measured on each image by selecting a region of interest that included only soft tissue and completely excluded the tumor (E.K.). The relative enhancement of this region of interest was computed by using the same methods as those described for computing the relative enhancement of the tumor.

For enhanced visibility of the images for publication, the radiographic images were histogram matched and sharpened by using unsharp masking. Both processes were performed by using the software. This processing was performed for display of the images only; the quantitative analysis was performed with the original unprocessed images.

Immunohistochemical Analysis and Histologic Evaluation of Explanted Tumors

For histologic examination, animals ($n = 2$) were injected at day 6 with the probe (455 mg of iodine per kilogram of

body weight) tagged with rhodamine. At 48 hours after injection, the animals were euthanized and the tumors were explanted. To visualize the tumor microvasculature, the tissue slices were immunohistochemically stained for the specific endothelial antigen CD31 (BD Biosciences Pharmingen, San Diego, Calif). The tissues also were stained with the nuclear stain 4',6-diamidine-2-phenylindole. The staining procedures followed established methods (24). The tumor sections were imaged at $\times 10$ with a microscope (Eclipse 80i; Nikon, Melville, NY) upright by using a charged-coupled device camera (Microfire; Optronics, Golate, Calif) that interfaced with the software (NeuroLucida; MicroBrightField Bioscience, Williston, Vt) to obtain a montage of each section. The histologic analysis was performed to verify the presence of extravascular intratumoral accumulation of the probe and its location with respect to the tumor vasculature (E.K.).

Data and Statistical Analysis

To determine the significance of the gray-level variation and tumor volumes among the various animal groups at different times, one-way analysis of variance with the post hoc Bonferroni test was performed (SPSS 15 for Windows; SPSS, Chicago, Ill). A *P* value of less than .05 was used to confirm significant differences at the 95% confidence level. The Anderson-Darling test was performed to verify that the data followed a normal distribution. The tumor growth enhancement profiles and tumor growth

curves were fitted into an exponential function (25) by using nonlinear regression (Levenberg-Marquardt algorithm) to compute the enhancement rate constant and the tumor growth rate constant, respectively (Polymath 5.0; Polymath Software, Willimantic, Conn). The area under the curve of the signal enhancement profiles was estimated by using the Gauss-Legendre orthogonal polynomial approximation. The correlation between the signal enhancement and the tumor growth rate was determined by using linear regression. Besides the Pearson product moment correlation, the correctness of the model was evaluated by examining the plots of the residuals and other statistical tests (SPSS 15 for Windows; SPSS).

Results

Imaging by Using a Clinical Mammography System

Figure 1 shows the modeled x-ray spectrum that resulted from the tube voltage and filter settings and the addition of the copper filter. With these operating conditions, the animal received an estimated radiation dose of 0.39 mGy per imaging session. In the pilot imaging sessions in which animals were injected with different doses of the probe, the threshold level for visualization of blood vessels was approximately 12 mg of iodine per milliliter in the blood (or a dose of 800 mg of iodine per kilogram).

For instance, although no vessels were visible before injection, they be-

came clearly visible in normal tissue and at the tumor 1 minute after injection of the probe at a dose of 1344 mg of iodine per kilogram, producing a concentration of approximately 20 mg of iodine per milliliter in blood (Fig 2). To eliminate signal from the blood vessels and probe the extravasation into the tumor, the dose selected for imaging after contrast agent administration was 455 mg of iodine per kilogram, producing a concentration of approximately 7 mg of iodine per milliliter in blood, a concentration less than the threshold level for detection of iodine in the blood. This allowed detection of the extravasated nanoprobe as early as 24 hours after injection, with no interference from the vascular signal (Fig 3). On the images obtained after injection, no blood vessels were visible in the normal tissue, whereas enhancement of the spleen, liver, and tumor could be clearly seen. Spleen and liver enhancement is consistent with clearance of liposomes via the reticuloendothelial system. Figure 4 shows two examples of how tumors were enhanced by the extravasated probe. The spatial and temporal variability of this enhancement, suggesting that each tumor had different tumor vasculature leakiness, could be clearly seen.

Histologic Evaluation of Extravasated Probe Tumor Distribution

The tumor was characterized by a highly vascularized peripheral rim and an internal core with low vascularization. The extravasated liposomes were localized in the well-vascularized periphery of the tumor in a patchy distribution (Fig 5).

Tumor Imaging

During the 3-day time of imaging, some tumors exhibited a rapid and substantial increase of enhancement, whereas other tumors showed a slow and low increase (Fig 6). Overall, the tumor enhancement displayed a variation among the animals, with the standard deviation of 55 digital units representing 50% of the mean value of 110 digital units 3 days after injection (Fig 6b). Although the tumor displayed substantial enhance-

Figure 1

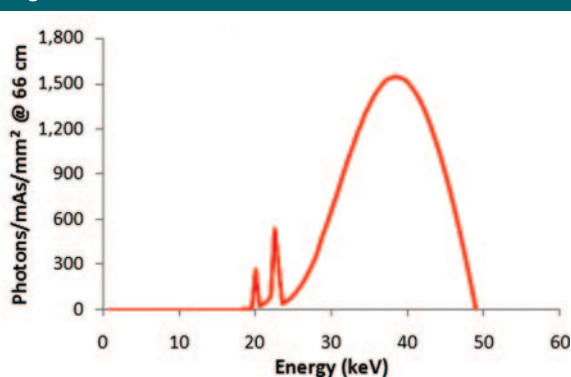


Figure 1: Graph shows estimation of 49-kVp rhodium/rhodium (0.025 mm of rhodium) x-ray spectrum with added 0.254-mm copper filter, according to simulation program.

ment, no enhancement was observed in normal tissues, confirming that the nanoprobe levels in the blood were below the detectable threshold level by using mammography. In contrast, tumors in the control group of rats that did not receive a contrast agent remained unenhanced, implying that no endogenous changes of the tumor tissue contributed to the enhancement.

Quantifying Treatment Effectiveness as a Function of Probe Extravasation

Liposomal doxorubicin slowed the progress of the tumor, displaying significant effectiveness 3 days after initiation of treatment, comparing control with treated groups (Fig 6c, 6d). The tumor response exhibited a variation, reflected by the tumor growth curve having standard deviations ranging from 10% to 35% of the mean value. Higher uptake of the probe by the tumor, indicating leakier vasculature, was associated with a slower tumor growth rate, suggesting a better therapeutic outcome with liposomal doxorubicin. Although the tumors of five animals grew marginally, the rest of the animals had to be euthanized

Figure 2

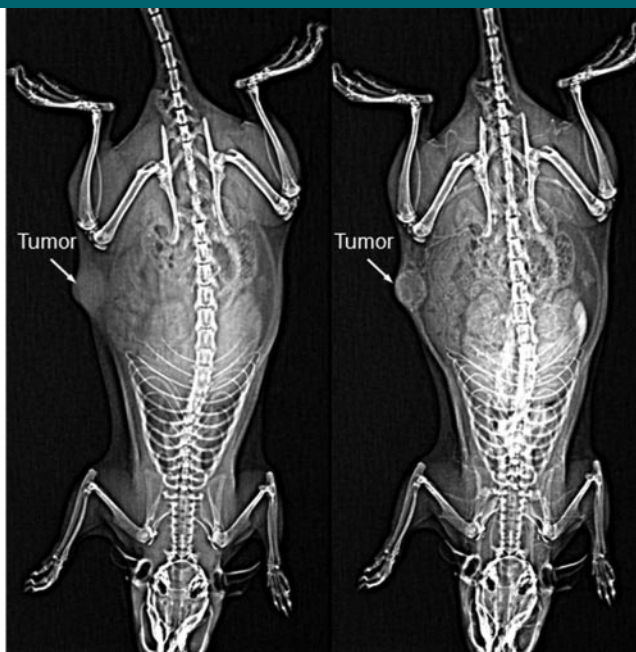


Figure 2: Whole-body images in rat with breast tumor in right flank obtained by using clinical digital mammography system. Left: Before administration of high dose (1344 mg of iodine per kilogram) of probe. Right: At 1 minute after. Administration resulted in vasculature visualization of tumor site and normal tissues.

Figure 3

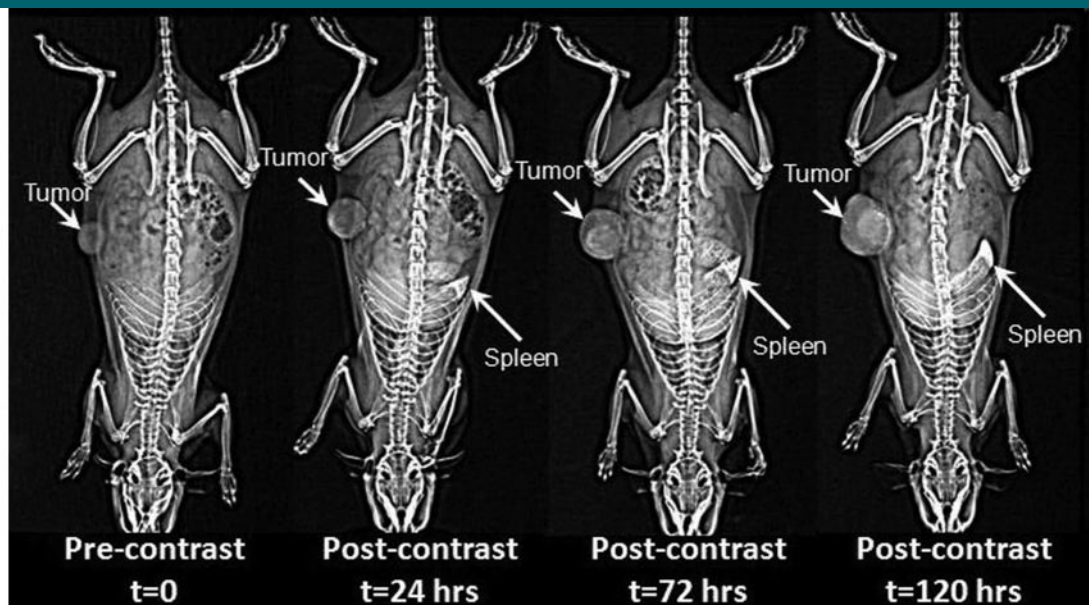


Figure 3: X-ray images display 5-day intratumoral fate of probe in rat breast tumor model before and 24, 72, and 120 hours after administration of probe at dose of 455 mg of iodine per kilogram. After injection, images showed that no blood vessels were visible in normal tissue; spleen, liver, and tumor were clearly seen.

because their tumors reached notably large sizes, which affected the quality of life of the animals.

We found a strong correlation be-

tween the tumor growth rate constant and the enhancement rate constant, with the less leaky tumors (low enhancement rate constant) having

faster tumor progress (high tumor growth rate constant) and vice versa (Fig 7). Besides the enhancement rate constant, the predictive power of other descriptive parameters, such as the area under the enhancement curve, were examined, displaying similarly good correlations ($R^2 = 0.856$). A better therapeutic outcome was observed in the good-prognosis subgroup from day 12 when compared with the untreated and the bad-prognosis subgroups. The bad-prognosis subgroup still benefited from the liposomal therapy, showing decreased tumor growth after day 14 when compared with the untreated control group.

Figure 4

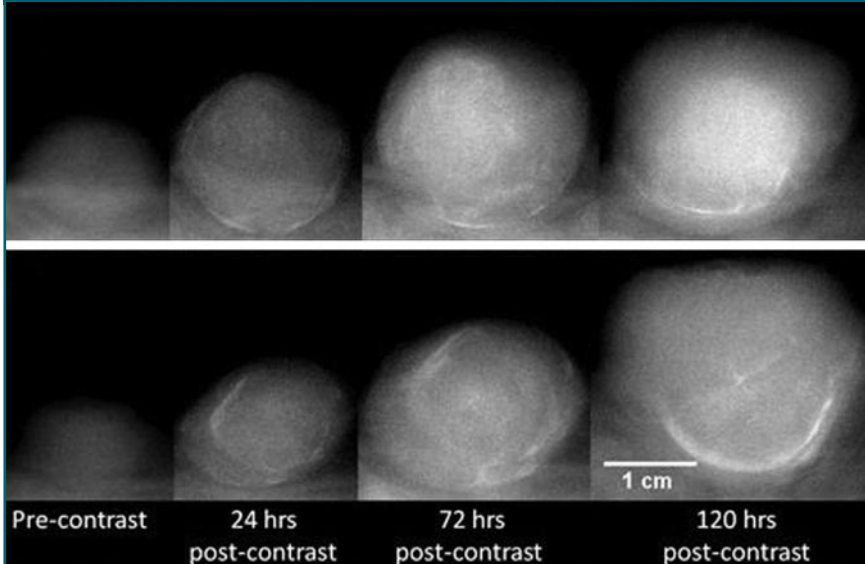


Figure 4: X-ray images of two tumors before and after injection of probe at dose of 455 mg of iodine per kilogram. Top: Tumor A. Bottom: Tumor B. Signal enhancement, in terms of gray levels, of tumor A is higher than that of tumor B by 40 and 70 digital units at 72 and 120 hours after injection, respectively; difference is clearly visible.

Discussion

The variability in tumor enhancement found in our study is consistent with that in a published study in which the standard deviation of the accumulation of liposomal doxorubicin in a rat brain tumor was 150% of the mean value (23). Numerous studies with liposomal doxorubicin conducted in mouse models of invasive and well-

Figure 5

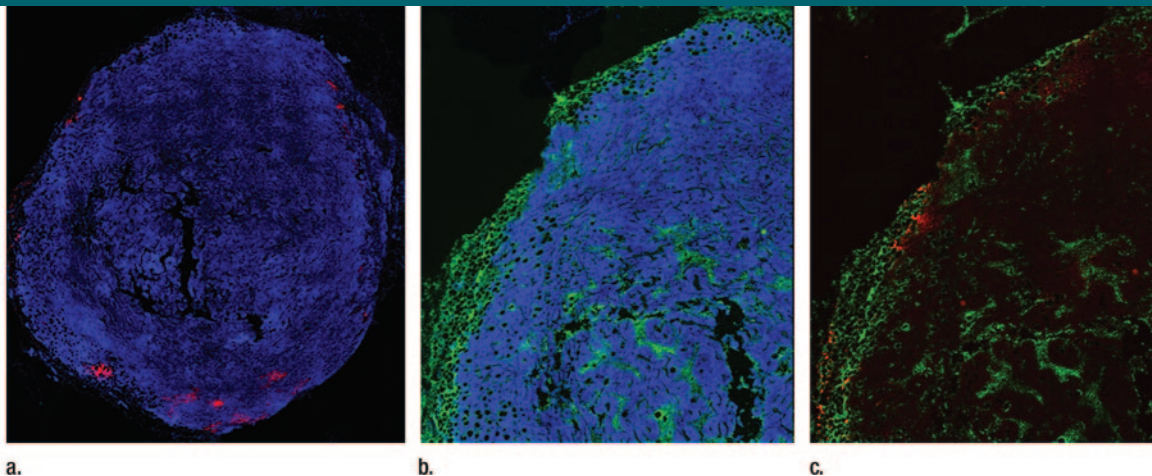
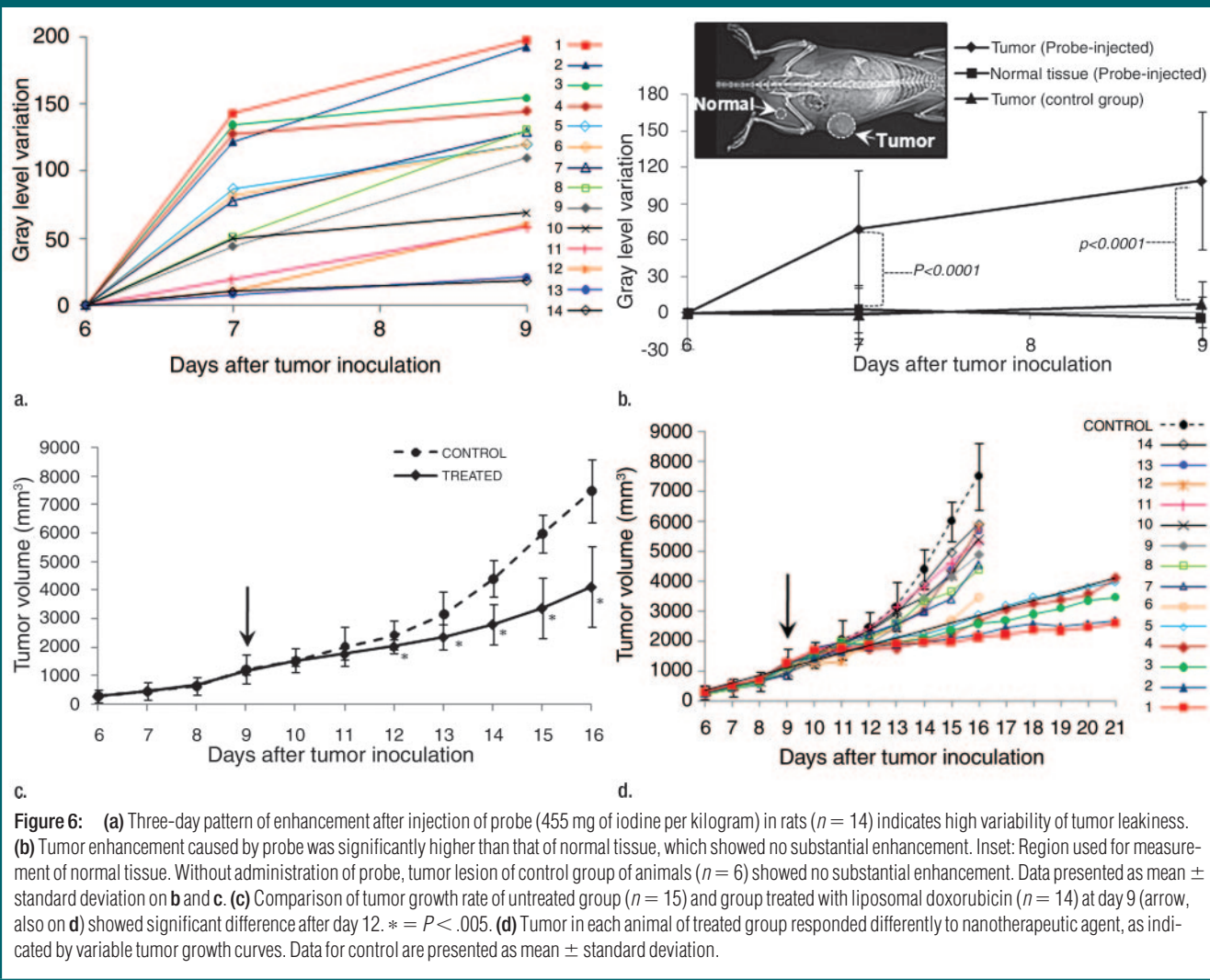


Figure 5: Fluorescent microscopy revealed microdistribution of probe in breast tumor lesion 48 hours after intravascular injection of rhodamine-tagged iodinated liposomes (red dots). (a) Liposomes localized in periphery of tumor, showing patchy distribution and blue staining. (4',6-Diamidino-2-phenylindole nuclear stain; original magnification, $\times 10$.) (b) Immunohistochemical microvascular staining was achieved by staining for specific endothelial antigen CD31 (green), revealing highly vascularized peripheral rim and less vascularized inner core. Top left quadrant of lesion is shown. (Original magnification, $\times 10$.) (c) In same histologic slice, probe was localized in well-vascularized rim. (CD31 [green] and rhodamine-liposome [red]; original magnification, $\times 10$.)

Figure 6



vascularized tumor xenografts have shown substantial variation in intratumoral accumulation and antitumor effects (26–30). Besides animal studies, the biodistribution of radiolabeled liposomes was studied in cancer patients, showing a considerable heterogeneity of the liposomal intratumoral deposition between different cancer types and between patients with the same tumor type (31). However, no attempt was made in that study to correlate the efficiency of a subsequent liposomal doxorubicin treatment.

The variability of the intratumoral contrast agent uptake captured during

the 3-day imaging sessions provided an accurate prognosis of the effect of liposomal doxorubicin on tumor growth rate. Because the timescale of extravasation of nanocarriers such as liposomal doxorubicin to tumors is on the order of a few days, the 3-day-imaging-derived enhancement rate constant correlated well with the tumor growth. The variable tumor response to the treatment observed in our study is consistent with human breast tumor xenografts in nude mice treated with liposomal doxorubicin, where the tumor growth curve had standard deviations of about 30% of

the mean value (26). The variability of tumor response to treatment depends on the type and the status of the tumor when treatment is initiated. Even in the aggressive model (32) used in our study, in which imaging was used to probe the vascular permeability of a tumor growing at a fast rate, the prognosis and antitumor effect of liposomal doxorubicin were significantly correlated.

Consistent with results in earlier reports (12,27,33), the liposomes showed a patchy distribution concentrated in the periphery of the tumor, where there is high vascularization,

associated with high levels of angiogenic and permeability factors (34,35).

It is important to note that the goal of our study was not to induce regression but to be able to noninvasively probe the enhanced permeation and retention effect status of a given tumor in a given animal and to correlate this status to the extent of change in tumor growth rate with administration of systemic nanotherapeutic agents. In this aggressive tumor model, the protocol to induce regression of tumor would require multiple injections of systemic nanotherapeutic agents, but this requirement would obfuscate the goals of the study, which were to facilitate non-invasive probing of the enhanced permeation and retention effect status of tumors to predict the degree of extravasation of systemically administered nanotherapeutic agents.

A limitation of our study was that the feasibility of the predictive capability of the nanoprobe was demonstrated

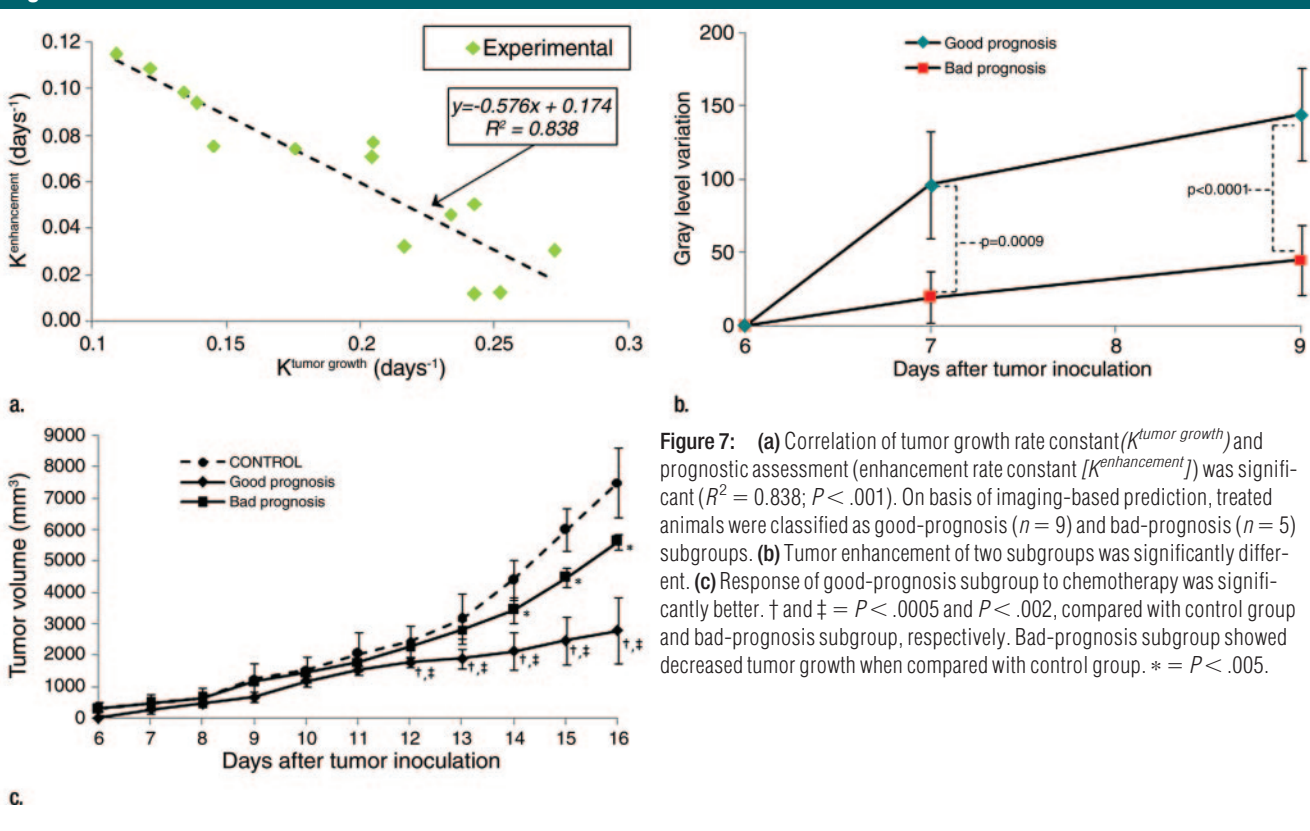
in a single-tumor model, although human cancer as a disease is much more heterogeneous than one experimental tumor model in terms of both tumors and hosts. Further testing in more tumor models is required to fully assess the value of this approach in clinical practice.

In summary, the extravasation of the nanoprobe was probed in a rat breast tumor by using a clinical mammography unit, and the animals were subsequently treated with liposomal doxorubicin of similar composition and particle size as the probe and as the clinically used liposomal chemotherapy to evaluate the predictive effectiveness of the probe. Imaging allowed the identification of good-prognosis and bad-prognosis subgroups prior to treatment. These subgroups demonstrated differential tumor growth rates after administration of the therapeutic agent. Our study demonstrates a contrast agent with the potential of helping to predict

the therapeutic outcome of a clinically used nanoparticle-based chemotherapeutic agent. Taking into consideration the idea that mammography prevails as the only method of low-cost mass screening of the general population for nonpalpable breast cancer, the visualization of the extravascular accumulation of the probe and, at the same time, the invisibility of the vasculature makes mammography an attractive noninvasive method for prediction of the outcome of cancer therapy. Finally, in our study, although planar x-ray imaging enabled prognosis by employing a clinically relevant breast cancer imaging modality, mammography, we hypothesize that such a strategy would also be possible with tomographic methods (eg, computed tomography), yielding further insights.

Practical application: Prediction of systemic liposomal chemotherapeutic effectiveness with iodinated liposomal probes and clinical digital mammogra-

Figure 7



phy would facilitate personalized treatment of breast cancer.

References

- Ferrari M. Cancer nanotechnology: opportunities and challenges. *Nat Rev Cancer* 2005; 5(3):161-171.
- Service RF. Materials and biology: nanotechnology takes aim at cancer. *Science* 2005; 310(5751):1132-1134.
- Gradishar WJ, Tjulandin S, Davidson N, et al. Phase III trial of nanoparticle albumin-bound paclitaxel compared with polyethylated castor oil-based paclitaxel in women with breast cancer. *J Clin Oncol* 2005; 23(31):7794-7803.
- Lasic DD. Doxorubicin in sterically stabilized liposomes. *Nature* 1996;380(6574):561-562.
- Yezhelyev MV, Gao X, Xing Y, Al-Hajj A, Nie S, O'Regan RM. Emerging use of nanoparticles in diagnosis and treatment of breast cancer. *Lancet Oncol* 2006;7(8):657-667.
- Lasic DD, Papahadjopoulos D. Liposomes revisited. *Science* 1995;267(5202):1275-1276.
- U.S. National Institutes of Health. ClinicalTrials.gov Web site. <http://www.clinicaltrials.gov/>. Accessed December 12, 2007.
- Folkman J. Angiogenesis in cancer, vascular, rheumatoid and other disease. *Nat Med* 1995;1(1):27-31.
- Carmeliet P, Jain RK. Angiogenesis in cancer and other diseases. *Nature* 2000; 407(6801):249-257.
- Maeda H. SMANCS and polymer-conjugated macromolecular drugs: advantages in cancer chemotherapy. *Adv Drug Deliv Rev* 2001; 46(1-3):169-185.
- Maeda H, Wu J, Sawa T, Matsumura Y, Hori K. Tumor vascular permeability and the EPR effect in macromolecular therapeutics: a review. *J Control Release* 2000;65(1-2):271-284.
- Yuan F, Leunig M, Huang SK, Berk DA, Papahadjopoulos D, Jain RK. Microvascular permeability and interstitial penetration of sterically stabilized (stealth) liposomes in a human tumor xenograft. *Cancer Res* 1994; 54(13):3352-3356.
- Wolff AC. Liposomal anthracyclines and new treatment approaches for breast cancer. *Oncologist* 2003;8(suppl 2):25-30.
- Fukumura D, Jain RK. Tumor microenvironment abnormalities: causes, consequences, and strategies to normalize. *J Cell Biochem* 2007;101(4):937-949.
- Hobbs SK, Monsky WL, Yuan F, et al. Regulation of transport pathways in tumor vessels: role of tumor type and microenvironment. *Proc Natl Acad Sci U S A* 1998; 95(8):4607-4612.
- Yuan F, Chen Y, Dellian M, Safabakhsh N, Ferrara N, Jain RK. Time-dependent vascular regression and permeability changes in established human tumor xenografts induced by an anti-vascular endothelial growth factor/vascular permeability factor antibody. *Proc Natl Acad Sci U S A* 1996;93(25): 14765-14770.
- Mukundan S Jr, Ghaghada KB, Badea CT, et al. A liposomal nanoscale contrast agent for preclinical CT in mice. *AJR Am J Roentgenol* 2006;186(2):300-307.
- Hubbell JH, Seltzer SM. Tables of x-ray mass attenuation coefficients and mass energy-absorption coefficients. <http://physics.nist.gov/PhysRefData/XrayMassCoef/cover.html>. Accessed December 5, 2007.
- Ullman G, Sandborg M, Dance DR, Yaffe M, Alm Carlsson G. A search for optimal x-ray spectra in iodine contrast media mammography. *Phys Med Biol* 2005;50(13):3143-3152.
- Flynn MJ, Samei E. Experimental comparison of noise and resolution for 2k and 4k storage phosphor radiography systems. *Med Phys* 1999;26(8):1612-1623.
- Sechopoulos I, Suryanarayanan S, Vedantham S, D'Orsi C, Karellas A. Computation of the glandular radiation dose in digital tomosynthesis of the breast. *Med Phys* 2007;34(1):221-232.
- Boone JM. Normalized glandular dose (DgN) coefficients for arbitrary X-ray spectra in mammography: computer-fit values of Monte Carlo derived data. *Med Phys* 2002; 29(5):869-875.
- McNeeley KM, Annapragada A, Bellamkonda RV. Decreased circulation time offsets increased efficacy of PEGylated nanocarriers targeting folate receptors of glioma. *Nanotechnology* 2007; 18:385101.
- Jain A, Kim YT, McKeon RJ, Bellamkonda RV. In situ gelling hydrogels for conformal repair of spinal cord defects, and local delivery of BDNF after spinal cord injury. *Biomaterials* 2006;27(3):497-504.
- Brown BW, Atkinson EN, Bartoszynski R, Thompson JR, Montague ED. Estimation of human tumor growth rate from distribution of tumor size at detection. *J Natl Cancer Inst* 1984;72(1):31-38.
- Park JW, Hong K, Kirpotin DB, et al. Anti-HER2 immunoliposomes: enhanced efficacy attributable to targeted delivery. *Clin Cancer Res* 2002;8(4):1172-1181.
- Kirpotin DB, Drummond DC, Shao Y, et al. Antibody targeting of long-circulating lipidic nanoparticles does not increase tumor localization but does increase internalization in animal models. *Cancer Res* 2006;66(13): 6732-6740.
- Saucier JM, Yu J, Gaikwad A, Coleman RL, Wolf JK, Smith JA. Determination of the optimal combination chemotherapy regimen for treatment of platinum-resistant ovarian cancer in nude mouse model. *J Oncol Pharm Pract* 2007;13(1):39-45.
- Drummond DC, Meyer O, Hong K, Kirpotin DB, Papahadjopoulos D. Optimizing liposomes for delivery of chemotherapeutic agents to solid tumors. *Pharmacol Rev* 1999; 51(4):691-743.
- Karathanasis E, Chan L, Balusu SR, et al. Multifunctional nanocarriers for mammographic quantification of tumor dosing and prognosis of breast cancer therapy. *Biomaterials* 2008;29:4815-4822.
- Harrington KJ, Mohammadtaghi S, Uster PS, et al. Effective targeting of solid tumors in patients with locally advanced cancers by radiolabeled pegylated liposomes. *Clin Cancer Res* 2001;7(2):243-254.
- Parish CR, Freeman C, Brown KJ, Francis DJ, Cowden WB. Identification of sulfated oligosaccharide-based inhibitors of tumor growth and metastasis using novel in vitro assays for angiogenesis and heparanase activity. *Cancer Res* 1999;59(14):3433-3441.
- Huang SK, Lee KD, Hong K, Friend DS, Papahadjopoulos D. Microscopic localization of sterically stabilized liposomes in colon carcinoma-bearing mice. *Cancer Res* 1992; 52(19):5135-5143.
- Damert A, Machein M, Breier G, et al. Up-regulation of vascular endothelial growth factor expression in a rat glioma is conferred by two distinct hypoxia-driven mechanisms. *Cancer Res* 1997;57(17):3860-3864.
- Takano S, Yoshii Y, Kondo S, et al. Concentration of vascular endothelial growth factor in the serum and tumor tissue of brain tumor patients. *Cancer Res* 1996;56(9):2185-2190.

Radiology 2009

This is your reprint order form or pro forma invoice

(Please keep a copy of this document for your records.)

Reprint order forms and purchase orders or prepayments must be received 72 hours after receipt of form either by mail or by fax at 410-820-9765. It is the policy of Cadmus Reprints to issue one invoice per order.

Please print clearly.

Author Name _____
Title of Article _____
Issue of Journal _____ Reprint # _____ Publication Date _____
Number of Pages _____ KB# _____ Symbol Radiology
Color in Article? Yes / No (Please Circle)

Please include the journal name and reprint number or manuscript number on your purchase order or other correspondence.

Order and Shipping Information

Reprint Costs (Please see page 2 of 2 for reprint costs/fees.)

_____ Number of reprints ordered \$ _____
_____ Number of color reprints ordered \$ _____
_____ Number of covers ordered \$ _____
Subtotal \$ _____
Taxes \$ _____

(Add appropriate sales tax for Virginia, Maryland, Pennsylvania, and the District of Columbia or Canadian GST to the reprints if your order is to be shipped to these locations.)

First address included, add \$32 for
each additional shipping address \$ _____

TOTAL \$ _____

Shipping Address (cannot ship to a P.O. Box) Please Print Clearly

Name _____
Institution _____
Street _____
City _____ State _____ Zip _____
Country _____
Quantity _____ Fax _____
Phone: Day _____ Evening _____
E-mail Address _____

Additional Shipping Address* (cannot ship to a P.O. Box)

Name _____
Institution _____
Street _____
City _____ State _____ Zip _____
Country _____
Quantity _____ Fax _____
Phone: Day _____ Evening _____
E-mail Address _____

* Add \$32 for each additional shipping address

Payment and Credit Card Details

Enclosed: Personal Check _____
Credit Card Payment Details _____
Checks must be paid in U.S. dollars and drawn on a U.S. Bank.
Credit Card: VISA Am. Exp. MasterCard
Card Number _____
Expiration Date _____
Signature: _____

Please send your order form and prepayment made payable to:

Cadmus Reprints

P.O. Box 751903

Charlotte, NC 28275-1903

Note: Do not send express packages to this location, PO Box.

FEIN #: 541274108

Signature _____ Date _____

Signature is required. By signing this form, the author agrees to accept the responsibility for the payment of reprints and/or all charges described in this document.

Invoice or Credit Card Information

Invoice Address Please Print Clearly

Please complete Invoice address as it appears on credit card statement

Name _____
Institution _____
Department _____
Street _____
City _____ State _____ Zip _____
Country _____
Phone _____ Fax _____
E-mail Address _____

Cadmus will process credit cards and Cadmus Journal Services will appear on the credit card statement.

If you don't mail your order form, you may fax it to 410-820-9765 with your credit card information.

Radiology 2009

Black and White Reprint Prices

Domestic (USA only)						
# of Pages	50	100	200	300	400	500
1-4	\$239	\$260	\$285	\$303	\$323	\$340
5-8	\$379	\$420	\$455	\$491	\$534	\$572
9-12	\$507	\$560	\$651	\$684	\$748	\$814
13-16	\$627	\$698	\$784	\$868	\$954	\$1,038
17-20	\$755	\$845	\$947	\$1,064	\$1,166	\$1,272
21-24	\$878	\$985	\$1,115	\$1,250	\$1,377	\$1,518
25-28	\$1,003	\$1,136	\$1,294	\$1,446	\$1,607	\$1,757
29-32	\$1,128	\$1,281	\$1,459	\$1,632	\$1,819	\$2,002
Covers	\$149	\$164	\$219	\$275	\$335	\$393

Color Reprint Prices

Domestic (USA only)						
# of Pages	50	100	200	300	400	500
1-4	\$247	\$267	\$385	\$515	\$650	\$780
5-8	\$297	\$435	\$655	\$923	\$1194	\$1467
9-12	\$445	\$563	\$926	\$1,339	\$1,748	\$2,162
13-16	\$587	\$710	\$1,201	\$1,748	\$2,297	\$2,843
17-20	\$738	\$858	\$1,474	\$2,167	\$2,846	\$3,532
21-24	\$888	\$1,005	\$1,750	\$2,575	\$3,400	\$4,230
25-28	\$1,035	\$1,164	\$2,034	\$2,986	\$3,957	\$4,912
29-32	\$1,186	\$1,311	\$2,302	\$3,402	\$4,509	\$5,612
Covers	\$149	\$164	\$219	\$275	\$335	\$393

International (includes Canada and Mexico)						
# of Pages	50	100	200	300	400	500
1-4	\$299	\$314	\$367	\$429	\$484	\$546
5-8	\$470	\$502	\$616	\$722	\$838	\$949
9-12	\$637	\$687	\$852	\$1,031	\$1,190	\$1,369
13-16	\$794	\$861	\$1,088	\$1,313	\$1,540	\$1,765
17-20	\$963	\$1,051	\$1,324	\$1,619	\$1,892	\$2,168
21-24	\$1,114	\$1,222	\$1,560	\$1,906	\$2,244	\$2,588
25-28	\$1,287	\$1,412	\$1,801	\$2,198	\$2,607	\$2,998
29-32	\$1,441	\$1,586	\$2,045	\$2,499	\$2,959	\$3,418
Covers	\$211	\$224	\$324	\$444	\$558	\$672

International (includes Canada and Mexico)						
# of Pages	50	100	200	300	400	500
1-4	\$306	\$321	\$467	\$642	\$811	\$986
5-8	\$387	\$517	\$816	\$1,154	\$1,498	\$1,844
9-12	\$574	\$689	\$1,157	\$1,686	\$2,190	\$2,717
13-16	\$754	\$874	\$1,506	\$2,193	\$2,883	\$3,570
17-20	\$710	\$1,063	\$1,852	\$2,722	\$3,572	\$4,428
21-24	\$1,124	\$1,242	\$2,195	\$3,231	\$4,267	\$5,300
25-28	\$1,320	\$1,440	\$2,541	\$3,738	\$4,957	\$6,153
29-32	\$1,498	\$1,616	\$2,888	\$4,269	\$5,649	\$7,028
Covers	\$211	\$224	\$324	\$444	\$558	\$672

Minimum order is 50 copies. For orders larger than 500 copies, please consult Cadmus Reprints at 800-407-9190.

Reprint Cover

Cover prices are listed above. The cover will include the publication title, article title, and author name in black.

Shipping

Shipping costs are included in the reprint prices. Domestic orders are shipped via FedEx Ground service. Foreign orders are shipped via a proof of delivery air service.

Multiple Shipments

Orders can be shipped to more than one location. Please be aware that it will cost \$32 for each additional location.

Delivery

Your order will be shipped within 2 weeks of the journal print date. Allow extra time for delivery.

Tax Due

Residents of Virginia, Maryland, Pennsylvania, and the District of Columbia are required to add the appropriate sales tax to each reprint order. For orders shipped to Canada, please add 7% Canadian GST unless exemption is claimed.

Ordering

Reprint order forms and purchase order or prepayment is required to process your order. Please reference journal name and reprint number or manuscript number on any correspondence. You may use the reverse side of this form as a proforma invoice. Please return your order form and prepayment to:

Cadmus Reprints
P.O. Box 751903
Charlotte, NC 28275-1903

Note: Do not send express packages to this location, PO Box. FEIN #: 541274108

Please direct all inquiries to:

Rose A. Baynard
800-407-9190 (toll free number)
410-819-3966 (direct number)
410-820-9765 (FAX number)
baynardr@cadmus.com (e-mail)

Reprint Order Forms and purchase order or prepayments must be received 72 hours after receipt of form.